The atmospheric continuum in the "terahertz gap" region (15–700 cm–1): Review of experiments at SOLEIL synchrotron and modeling

T.A. Odintsova, A.O. Koroleva, A.A. Simonova, A. Campargue, M.Yu. Tretyakov

The atmospheric continuum in the "terahertz gap" (15-700 cm^{-1}): review of experiments at SOLEIL synchrotron and modeling

T. A. Odintsova[1], A. O. Koroleva[1], A. A. Simonova[2], A. Campargue[3], and M. Yu. Tretyakov[1]

[1] *Institute of Applied Physics of RAS, Nizhniy Novgorod, Russia*
[2]*V.E. Zuev Institute of Atmospheric Optics SB RAS, Tomsk, Russia*
[3]*Univ. Grenoble Alpes, CNRS, LIPhy, Grenoble, France*

Key words: SOLEIL synchrotron, atmospheric continuum, THz gap, dimer, far wings

Abstract

The results of our recent water vapor related continuum studies in the range of the "terahertz gap" at the AILES beam line of the SOLEIL synchrotron using Fourier transform spectrometer are reviewed and summarized. The continuum of pure water vapor and its mixture with N_2, O_2 and dry air were investigated in the 15 – 700 cm^{-1} range in conditions close to atmospheric. Analysis of the frequency and temperature dependence of the self-continuum revealed a significant contribution of stable water dimer to the observed absorption, which is not taken into account by the MT_CKD semi-empirical model of the continuum, widely used for atmospheric applications. We propose a physically based approach for the continuum modeling, which accounts explicitly for the contribution of dimers and far wings of monomer resonance lines. We applied the suggested approach for the water vapor self-continuum modeling in the H_2O rotational band and sustained it by comparison to the SOLEIL data. The frequency dependence of the relative contributions of far wings, stable and metastable dimers to the self-continuum is evaluated. Prospects for further developments of the atmospheric continuum modeling are given.

1. Introduction

In spite of recent progress, the terahertz frequency range (0.3 – 10 THz or 10 – 300 cm^{-1}) remains poorly studied, mostly due to the lack of available radiation sources and receivers. Due to this reason and its location between the microwave and infrared ranges, it is called the "terahertz gap" (see reviews in [Sizov_2010, Consolino_2017] and references therein). The THz gap is interesting because it contains absorption spectra of many astrophysical, organic and atmospheric molecules. For example, significant lines of the pure rotational absorption spectrum of water vapor extends to a frequency of about 18 THz (600 cm^{-1}), *i.e.* the main part of the band falls into the THz gap. In addition, the maximum of outgoing heat flux of the Earth falls in the THz range. The development of high-speed wireless communication systems in the THz range requires taking into account atmospheric absorption, mainly due to water vapor. Also, to model accurately the Earth's radiation balance it is necessary to take into account the atmosphere absorption, in particular, water vapor absorption.

The absorption of electromagnetic radiation by water vapor – the main greenhouse gas in the Earth's atmosphere – is traditionally subdivided into two components, namely, the *resonance absorption* (the sum of the absorption lines, corresponding to roto-vibrational transitions of water monomers) and the smoothly varying with frequency *continuum absorption*, or just the continuum (absorption under the resonance lines). The resonance absorption has been much better characterized both theoretically and experimentally than the continuum. This is due *(i)* to the difficulty to measure accurately weak continuum absorption and *(ii)* to the fact that the continuum is determined as a difference between experimental water vapor absorption and calculated resonance absorption spectrum and, therefore, strongly depends on the line shape model and on the accuracy of its parameters. Compared to the resonance absorption, the relative magnitude of the continuum strongly varies: the continuum can be several orders of magnitude weaker than the resonance absorption near the line center and by one order of magnitude (and even more) stronger in between H_2O lines (the so-called "atmospheric" microwindows). The water vapor continuum has to be accounted for in radiative transfer codes modeling our atmosphere. Currently, a semi-empirical continuum model – the MT_CKD [MT_CKD] is widely used for atmospheric applications. Our recent experimental studies [Odintsova_2017, Odintsova_2019, Odintsova_2020, Koroleva_2021] have been motivated by the need to validate the MT_CKD continuum model in the THz range. In addition these new data may give new insights on the physical origin of the continuum and serve as the basis for a physically based continuum modeling in a wide range of frequencies and thermodynamic conditions. It is well known that the continuum arises from

the collisional interaction of molecules [Vigasin_2003], in particular, *pair interactions* because triple effects can be neglected at atmospheric conditions. Thus, the continuum magnitude varies as the product of interacting molecules concentrations (or partial pressures).

The atmospheric continuum consists of a dry and a wet component. The *dry continuum* arises mainly from the interaction of nitrogen and oxygen molecules. The *wet continuum* is related to atmospheric water vapor and arises from the interaction of water molecules with each other (*self-continuum*) and with other atmospheric molecules (*foreign-continuum*). Pair interaction of molecules leads to *(i)* the formation of bimolecular states including metastable (quasibound) and stable (truly bound) dimers and free-pair states (the latter is known to be dominant contributor to the dry continuum [Vigasin_2003, Bissolles_2003, Serov_Balashov_2020] but provides negligible contribution in pure water vapor at usual atmospheric conditions [Vigasin_1991, Leforestier_2010, Tretyakov_2015]) and *(ii)* the deviation of the far wings of "observed" water lines from theoretical profiles derived in the impact approximation [Ma_Tipping_Leforestier_2008, Elsasser_1938, Serov_Odintsova_2017]. Each continuum component varies smoothly with frequency, which makes complicated to disentangle the two contributions. Two complementary hypotheses on the continuum origin, based on the two aforementioned mechanisms have been suggested for a long time. The hypothesis of the dominant role of far wings of water lines is supported by the fact that sophisticated [Tvorogov_Nesmelova_1994, Klimeshina_2015] or semi-empirical [Clough_1989] modification of line profile at large detuning from the line center were able to empirically account for the scarce experimental data at disposal. This approach constitutes the basis of the MT_CKD model [MT_CKD]. However, as demonstrated in [Tretyakov_Serov_2013] and in subsequent study [Serov_Koshelev_2014], spectral features observed in the continuum in the mm-submm wave range (0.1-0.26 THz or 3.5-8.7 cm^{-1}) can be unambiguously attributed to the stable water dimer absorption. Moreover, quantitative evaluation of the dimer absorption led to the conclusion that this mechanism is dominant in water vapor continuum in this spectral range. Evidence of stable water dimer absorption within H_2O fundamental vibrational bands was also demonstrated [Ptashnik_2011, Birk_2020]. It should be mentioned that different continuum constituents are expected to have different temperature dependence [Vigasin_1991] which could help to discriminate them. These facts form the general theoretical ground for the analysis of the continuum composition.

The THz range is very attractive for studying the continuum, mainly because the results of global sophisticated *ab initio* calculations of the bound water dimer spectrum are available

in this region [Scribano_2007]. All possible rotational-vibrational tunneling transitions of the dimer up to its first dissociation limit are explicitly taken into account in these calculations, contrary to the simplified calculations in the IR range (see e.g. [Kjaergaard_2008, Salmi_2008] and refs therein) which consider the dimer as two individually vibrating monomer units and neglect the low frequency modes involving both molecules (only band centers and band intensities are calculated). The detailed knowledge of the dimer spectrum in the THz range is expected to help to evaluate other physical mechanisms contributing to the measured continuum.

For quantitative spectroscopic studies of the continuum absorption in the THz range, a powerful radiation source operating in a broad frequency range is needed. Keeping in mind the characteristic scale of the continuum variation with frequency (hundreds of GHz), the desired operating range of the source should cover tens of THz. The high power, large spectral coverage and high stability of the SOLEIL synchrotron make it an ideal source for this kind of studies.

Since 2014, several experimental campaigns have been organized (SOLEIL Projects Nos. 20140227, 20170067 and 20180347), aiming at studying the water vapor continuum in the frequency range of pure rotational water band (about 0.45 – 21 THz or 15 – 700 cm^{-1}). The results of the analysis of the recorded spectra together with obtained continuum cross-sections have been reported in a series of papers [Odintsova_2017, Odintsova_2019, Odintsova_2020, Koroleva_2021]. The present contribution summarizes conclusions of these investigations. Furthermore, the approach for physically based continuum modeling is outlined and is applied to the SOLEIL measurements of the self-continuum in the pure rotational water band. This allows making quite definite conclusions about bimolecular absorption and far wings contributions.

For the reader's convenience, we briefly recall in the next section, the main characteristics of the measurement method and the experimental conditions, and summarize the obtained experimental data. In the third section, we propose a physically based absorption model, which includes the continuum in a natural way and demonstrate the application of its simplified version to the THz region. In the conclusion, the main results of the trial are presented and prospects for further developments are given.

2. Experimental data

2.1 FTS recordings

Spectra were recorded at AILES beamline of SOLEIL synchrotron using a high–resolution Fourier-Transform spectrometer (Bruker IFS–125HR). Coherent radiation (CR) and standard (SR) synchrotron operation modes were used to cover the 15 – 35 cm^{-1} and 40 – 700 cm^{-1} spectral intervals, respectively. The summary of the various experimental conditions of the recordings is presented in **Table 1**. A multiple reflection cell with effective path length of 151.75 m was used. To record spectra at elevated temperature (326 K), the cell was wrapped with several 60 ºC silicon rubber heaters and additional thermal isolation. To evaluate and exclude possible bias due to a change of the base line related to the pressure variation, a two-steps procedure was adopted for the gas mixture. At the first step, the cell was filled with pure water vapor, and then a foreign gas was gradually added. At the second step, the resulting mixture was gradually pumped out. It was assumed that the water vapor pressure is constant during filling and decreases in proportion to the total mixture pressure during pumping out. The expected water content is generally confirmed by observed integrated intensities of unsaturated water lines determined from fitting their shape. It should be mentioned, that during the experimental studies no manifestation of the effects of adsorption-desorption of water in the cell was observed (that is evidenced by almost instantaneous stabilization of water vapor pressure after its injection), which is associated with a very large volume of the gas cell compared to its inner surface area.

Table 1. Experimental conditions of the various recordings and corresponding reference of their analysis

Sample	Frequency range, cm^{-1}	Water pressure, mbar	Total pressure mbar	*T*,K	Resolution, cm^{-1}	Number of spectra	Ref.
$H_2{}^{16}O$	15-35	11-16	11-16	296	0.02	2	[Odintsova2017, Odintsova2019]
$H_2{}^{18}O$	15-35	13-16	13-16	296	0.02	2	[Odintsova2019]
$H_2{}^{16}O$	40-700	3-16	3-16	296, 326	0.02, 0.002	25	[Odintsova2017, Odintsova2019, Odintsova2020]
$H_2{}^{18}O$	50-500	2-6	2-6	296	0.02, 0.002	10	[Odintsova2019]
$H_2{}^{16}O$ – air	50-500	4	200-400	296	0.02	9	[Koroleva2021]
$H_2{}^{16}O$ – N_2	50-500	2-4	20-430	296	0.02	9	[Koroleva2021]
$H_2{}^{16}O$ – O_2	50-500	4	200-400	296	0.02	9	[Koroleva2021]

2.2 Analysis and cross-section retrieval

The experimental transmittance, *T*, is related to the absorption coefficient, α, through the expression $T=\exp(-\alpha L)\otimes f_{app}$, where L and f_{app} are the absorption pathlength and the

apparatus spectral resolution function, respectively. The FTS spectra were analyzed using commonly accepted approach: the difference between measured (α) and the calculated resonance (α_R) absorption coefficients is referred to the continuum (α_C):

$$\alpha_C(\nu,T,P) = \alpha(\nu,T,P) - \alpha_R(\nu,T,P), \quad (1)$$

where ν, P and T are frequency, pressure and temperature, correspondingly. Resonance absorption was modeled as a line-by-line sum using the HITRAN line list for 6 most abundant water isotopologues [HITRAN2016] and Van Vleck–Huber line profile [VanWleck_Huber_1977, Clough_1989]. The standard far-wing cut-off at 25 cm^{-1} from the line center was applied, the far wings of the line below and above the cut-off frequency being excluded and the remaining almost rectangular absorption (the "pedestal" or "plinth") underneath the modeled line profile being preserved as an intrinsic part of the resonance absorption. Note that a different choice is made in the MT_CKD model for which the plinth is considered as part of the continuum. It should be mentioned, that in the sub-THz frequency range (15 – 35 cm^{-1}), line shape parameters measured by microwave methods [Golubiatnikov_2006, Golubiatnikov_2005, Golubiatnikov_2008, Koshelev_2011, Koshelev_2007, Tretyakov_2013] were used instead of HITRAN values, when available. This allows us to determine the continuum practically in the whole spectral range recorded contrary to the majority of previous investigations in this range [Burch_1981, Podobedov_2008] and in the IR [Burch_1981, Burch_Alt_1984, Ptashnik_Shine_2011, Campargue_Kassi_2016], where it was determined only in points corresponding to microwindows of transparency due to the necessity of minimizing the contribution of line parameters uncertainties.

The continuum absorption coefficient can be written as the sum of the self- (α_{self}) and foreign- (α_{for}) continua:

$$\alpha_C(\nu,T,P) = \alpha_{self}(\nu,T,P) + \alpha_{for}(\nu,T,P)$$
$$= C_s(T)P_{H_2O}^2/k_BT + C_f(T)P_{H_2O}P_{for}/k_BT. \quad (2)$$

Here $C_s(T)$ and $C_f(T)$ are the self- and foreign-continuum cross-sections (in $cm^2molec^{-1}atm^{-1}$), k_B is Boltzmann constant, P_{H_2O} and P_{for} are water vapor and foreign gas partial pressure, respectively. For pure water vapor, only the first term of equation (2) remains.

The expected pressure dependences (Eq.2) of the continuum absorption were systematically checked confirming the reliability of the measurements (and in particular baseline stability): the continuum of pure water vapor increases quadratically with pressure (see e.g. Fig.1 of [Odintsova_2020]), the continuum of a mixture of water vapor with foreign gas was checked to increase linearly with the partial pressure of the added foreign gas (Fig.2

of [Koroleva_2021]) and to decrease as the square of the total pressure during the pumping out of the mixture (Fig.4 of [Koroleva_2021]). In 40 – 700 cm^{-1} spectral interval $C_s(T)$ and $C_f(T)$ values were derived from a fit of the pressure dependence obtained at about 200 spectral points located in microwindows of transparency. Let us note that, although less accurate, the C_s values retrieved from wet gas mixtures are consistent with the values obtained with pure water vapor [Koroleva_2021]. The $C_f(T)$ values obtained from the analysis of the data corresponding to filling and pumping stages are also in good agreement.

The air-continuum cross-section of atmospheric water vapor, $C_{f\text{-}air}$, was obtained by two ways. In the first one, $C_{f\text{-}air}$ was retrieved directly from experimental spectra of mixture of water vapor with dry atmospheric air (see [Koroleva_2021]). In the second one, $C_{f\text{-}air}$ was calculated from $C_{f\text{-}N2}$ and $C_{f\text{-}O2}$ values retrieved from spectra of water vapor with N_2 and O_2. Considering the dominant role of pair interactions and atmospheric abundances of major atmospheric gases N_2 (≈ 78%), O_2 (≈21%) and Ar (≈1%), $C_{f\text{-}air}$ can be expressed as:

$$C_{f\text{-}air}=0.78C_{f\text{-}N2}+0.21C_{f\text{-}O2}+0.01C_{f\text{-}Ar} \quad (4)$$

Since contributions of $C_{f\text{-}O2}$ and $C_{f\text{-}Ar}$ were found negligible [Koroleva_2021, Bauer_1998], $C_{f\text{-}air}$ reduces to:

$$C_{f\text{-}air}=0.78C_{f\text{-}N2} \quad (5)$$

The result agrees with the foreign-continuum retrieved from a mixture of H_2O with dry air [Koroleva2021]. Both, consistency of all experimental data sets with each-other and expected pressure dependences serve as a tough validation of obtained experimental data.

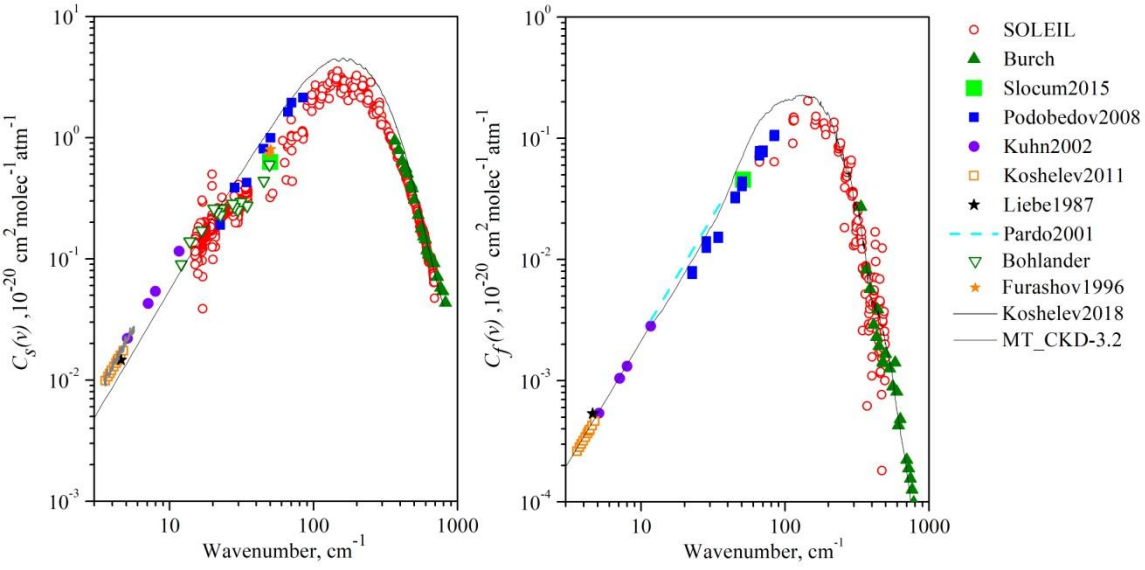

Fig. 1. Self- (left panel) and foreign- (right panel) continuum at 296 K: red circles: SOLEIL measurements [Odintsova_2020,Odintsova_2019, Odintsova_2017, Koroleva_2021], green

triangles: [Burch_1981, Burch_Alt_1984], blue squares: [Podobedov_2008], black star: [Liebe_1987], green empty triangles: measurements of R.A. Bohlander [Burch_1981], light green square: [Slocum_2015], violet circles: [Kuhn_2002], orange empty squares: [Koshelev_2011], orange star: [Furashov1996], grey curve: [Koshelev_2018], blue dash curve: [Pardo_2001], black curve: MT_CKD-3.2 model [MT_CKD].

Temperature dependence of continuum cross-section $C(T)$ is empirically approximated using power law [Koshelev_Serov_2011, Liebe_1897, Kuhn_2002]:

$$C_{s,f}(T)=C_{s,f}(T_0)\cdot(T_0/T)^n\,, \quad (6)$$

where T_0 = 296 K, and n is the temperature exponent. The temperature exponent n of the self-continuum was estimated from C_s at 296 K and 326 K [Odintsova_2020]. Since the temperature difference of the SOLEIL recordings was limited to 30 K, the above empirical law with one adjustable parameter was chosen instead of more complex functions (see, for example, [Ptashnik_2019], [Vigasin_2000]).

Figure 1 presents an overview comparison of the water vapor self- and foreign-continua measurements available in the literature to our data and to the MT_CKD-3.2 model at 296 K. Note that SOLEIL C_s values with estimated uncertainty higher than 15 % are not shown in **Figure 1**, the exception is low-frequency wing of the band (15-100 cm^{-1}), for which all available values are given (even with uncertainty higher than 50 %). SOLEIL data and their uncertainties are given in Supplementary Materials of our previous papers [Odintsova_2019, Odintsova_2020, Koroleva_2020]. We would like to point out that the spread of experimental points, which is seen in Fig. 1, is the best characteristic of their uncertainty, including systematic errors related, in particular, to uncertainty of resonance line parameters because the continuum is expected to be smooth due to its nature. Note that the estimated experimental uncertainty is often smaller that the spread of points. Overall, the SOLEIL results from [Odintsova_2017, Odintsova_2019, Odintsova_2020] and previous data [Podobedov_2008, Burch_1981, Koshelev_Serov_2011, Kuhn_2002, Liebe_1987, Slocum_2015, Furashov_1996] cover the whole range of the H_2O pure rotational band (significant lines of the band are spread from 0.7 up to about 600 cm^{-1}). Note that the continuum around the intensity maximum of the H_2O rotational band (which is located around 150 cm^{-1} and coincides with the intensity maximum of the continuum) – from 84 to 350 cm^{-1} – was not investigated earlier. Overall, using a wide variety of experimental conditions (pressure range, gas sample temperature, bolometer filter, synchrotron mode), our successive measurement campaigns at SOLEIL synchrotron allowed us collecting data covering the broad frequency range from 15 up to 700 cm^{-1} (with minor problems at the edges of the studied frequency range related to insufficient radiation power) and estimating the temperature dependence of

the self-continuum in the 84– 414 cm^{-1} region [Odintsova_2020]. Data of different campaigns are consistent with each other. Above 350 cm^{-1}, an excellent agreement with Burch's measurement is noted [Burch1981, Burch_Alt_1984]. In the 3.5– 84.1 cm^{-1} low-frequency range, several studies are available [Koshelev_2011, Kuhn_2002, Liebe_1987, Slocum_2015, Furashov_1996, Kwon_2021, Yang_2014, Podobedov_2008, Burch_1981]. Our C_s values in the 15 – 35 cm^{-1} range agree with the results of [Podobedov_2008, Burch_1981]. It is worth mentioning an encouraging agreement with unpublished results obtained by R. A. Bohlander and reported by Burch in 1981 [Burch_1981]. Our comparison does not consider the results reported by [Kwon_2021, Yang_2014] in the 10– 33 cm^{-1} range because these broad-band experimental data were fitted assuming purely quadratic frequency dependence of the continuum absorption, thus only the mean values of $C_s(\nu)$ and $C_f(\nu)$ were determined for the whole studied range. Some deviations of our self-continuum from literature data are observed in the range of 50.3– 84.1 cm^{-1}, where our $C_s(\nu)$ values are smaller than the values reported in [Podobedov_2008] and [Slocum_2015, Furashov_1996, Burch_1981] by a factor between 1.5 and 2. This deviation can be explained by uncertainty of experimental continuum: the uncertainty of SOLEIL's data coming from low signal-to-nose ratio of our spectra at the edge of the working range of SR synchrotron mode, and uncertainty of data of Podobedov [Podobedov2008] and Bohlander [Burch_1981], that is not reported, but can be estimated by spread of available data.

For proper comparison of our data with the MT_CKD model, the cumulative plinth of the H_2O rotational spectrum was subtracted from the model prediction (recall aforementioned convention in the calculation of the resonance line contribution). Although the general agreement with the MT_CKD-3.2 model is satisfactory (Fig. 1a), the detailed comparison reveals some deviations. The MT_CKD-3.2 model overestimates the self-continuum by about 30% near its maximum. The agreement gradually improves towards the edges of the H_2O band, which is not surprising because experimental results are used for updating the MT_CKD model. However, we note that, the model does not reproduce experimental frequency dependence of C_s in the mm and sub-mm wave range (3.5 – 50 cm^{-1}). At the lower (< 10 cm^{-1}) and upper (> 20 cm^{-1}) parts of this spectral range, the model systematically underestimates and overestimates the continuum, respectively.

As concerns the foreign-continuum cross-sections determined in the 60–500 cm^{-1} range, they are consistent with previous experimental studies available in the low- [Podobedov_2008, Pardo_2001, Koshelev_2011, Koshelev2018, Liebe_1987, Kuhn_2002, Kwon_2021, Yang_2014, Slocum_2015] and high-frequency [Burch_1981, Burch_Alt

_1984] wing of the H_2O band. Again, the MT_CKD-3.2 model shows a very good agreement below 50 cm^{-1} and above 200 cm^{-1}, although some overestimate is notable near the maximum of the band (60–200 cm^{-1}) where previous experimental data were absent.

3. Some insights on the origin of the water continuum

3.1. General outline of atmospheric continuum modeling

The semi-empirical MT_CKD model of the water continuum is the most widely used model for atmospheric applications [Alvarado_Payne_2013]. It covers the 0 – 20000 cm^{-1} frequency range and is updated periodically as a new reliable empirical data on the continuum become available (see for instance Fig. 8 of [Lechevallier_2018] for the infrared windows). The model is a *far wings model*. Resonance line wings modifying χ-factors are tuned to force agreement with observations, on the assumption that deviations are due to departures from the Lorentzian profile. The model does not take into account the absorption related to the collisional formation of pair molecular states (although this contribution, in particular, coming from free pairs and partly from metastable dimers might be partly included in an effective way in the frame of the approach adopted by the model). This might lead to notable differences in the frequency ranges where the contribution of the dimer absorption is significant. Such deviations were demonstrated in some in-band regions corresponding to fundamental intramolecular vibrational modes of stable water dimer and their overtones [Ptashnik_Shine_2011, Baranov_2011, Simonova_2022, Birk_2020]. They are also seen in the range of pure rotational band of water dimer (below 40 cm^{-1}) in Fig. 4 of [Odintsova_2019] and Fig. 8 of [Koshelev_2018].

In [Serov_Odintsova_2017], a general approach for a physical modeling of radiation absorption by atmospheric molecules was proposed. It explicitly takes into account all classes of absorbers that can be collisionally formed in a gas mixture and it does not require the introduction of the uncertain continuum term. We remind below the basic idea of this approach.

The traditionally defined continuum can be expressed in terms of the new approach as will be shown below. The general expression for the total absorption coefficient of a mixture of gases is commonly written as:

$$\alpha(\nu) = \alpha_1(\nu)\rho_1 + \alpha_2(\nu)\rho_2 + \alpha_3(\nu)\rho_3 + \ldots, \quad (7)$$

where $\alpha_1(\nu)$, $\alpha_2(\nu)$... are spectra of corresponding species normalized by their densities ρ_1, ρ_2.... Note that this linear equation is the basis of the traditional approach to the absorption

modeling, which neglects the collisional formation of molecular complexes (unaccounted absorbers) in gases and, therefore, misses the corresponding absorption. The resulting disagreement with observations leads to necessity of the continuum introduction. To fix the problem we take into account that monomers of real gas can be in monomolecular, bimolecular, trimolecular *etc*. states. So the complete exact equation for the total absorption coefficient in real gas (for clarity let us consider pure gas of identical molecules) looks exactly the same as Eq. (7) but now $\alpha_1(\nu)$, is the spectrum of monomers (in the units of absorption coefficient) normalized by number density of monomers or *monomolecular* absorption, $\alpha_2(\nu)$ is similarly the normalized absorption by molecular pairs or *bimolecular* absorption, $\alpha_3(\nu)$ is similarly trimolecular absorption, and ρ_1, ρ_2... are number densities of corresponding absorbers. It is obvious that at relatively low pressures when binary collision approximation is valid, the following relations hold: $\rho_1 = \rho - \rho_2 - \rho_3 - \ldots \approx \rho$, $\rho_2 = K_2\rho^2$ and $\rho_3 = K_3\rho^3$, where ρ is the total (including those in multimolecular states) number density of monomers, K_2 and K_3 are equilibrium constants of bimolecular and trimolecular states. Note that the presence of bimolecular and trimolecular states is taken into account in the virial equation of state of a gas by the second and the third virial coefficients, which values are related to equilibrium constants of bimolecular and trimolecular states [Tretyakov_Serov_2011]. Thus Eq. (7) is written as

$$\alpha(\nu) = \alpha_1(\nu)\rho + \alpha_2(\nu)K_2\rho^2 + \alpha_3(\nu)K_3\rho^3 + \ldots, \quad (8)$$

Note that each contribution (summand of Eq. (8)) may include resonance and non-resonance components. At the same time, the continuum in accordance with its common definition of Eq. (1), includes the total contribution of the second, third and subsequent summands and part of the first summand. Further minor complication of the equation is required for the adequate comparison between various components of absorption of our and traditional approaches. Continuum absorption usually characterized by cross-section (absorption coefficient normalized by product of molecular number density and pressure) in units of $cm^2molec^{-1}atm^{-1}$. These units come from resonance absorption modeling for variable quantity of absorbing molecules which involves integrated line intensity (normalized by molecular number density in $molec/cm^3$) and collisional line width (normalized by pressure in atm^{-1}). The total absorption (in cm^{-1}) can be written as:

$$\alpha(\nu) = \rho\,[\alpha_1(\nu) + \alpha_2(\nu)K_2\rho k_BT + \alpha_3(\nu)K_3\rho^2(k_BT)^2 + \ldots], \quad (9)$$

so α_1 and α_2 are in cm^2molec^{-1}, ρ is in $molec/cm^3$, K_2 and K_3 are in atm^{-1} and atm^{-2}, respectively. Note that the unit of K_2 is $(molec/cm^3)^{-1}$ in Eq.(8), and (atm^{-1}) in Eq. (9). Under atmospheric conditions the components of the Eq. (9) starting from the third are negligible [Tretyakov_Serov_2011]. Bimolecular components of the total absorption (Eq. (9)) can be written as:

$$K_2\,\alpha_2 = K_{BD}BD + K_{MD}\,MD + K_FF,\ K_2 = K_{BD} + K_{MD} + K_F, \qquad (10)$$

where *BD*, *MD* and *F* (in cm^2molec^{-1}) are spectra of dimers (stable and metastable) and of free pairs normalized by their density, K_{BD}, K_{MD} and K_F are stable and metastable dimers and free pairs equilibrium constants (in atm^{-1}), characterizing their partial pressures (in atm.) as $P_X = K_XP^2 = K_X(\rho kT)^2$, X=*BD, MD, F*. The approach cannot be fully implemented in the practical modeling (even within the pair molecular interaction approximation *i.e.* neglecting the third and all other summands) until sufficient theoretical description is developed for *(i)* bimolecular spectra related to major atmospheric constituents *i.e.* of H_2O-H_2O, H_2O-N_2, H_2O-O_2, N_2-N_2, N_2-O_2, O_2-O_2, H_2O-Ar, *etc*, including their free pairs and both stable and metastable dimeric states, and *(ii)* resonance line shape of monomers at large detuning from the line center. In this work, we follow this approach but substitute the missing data by empirical modeling. With these simplifications, we formulate here an alternative to the MT_CKD approach considering both the contributions of bimolecular absorption and far wings of monomer resonance lines. The region of the H_2O rotational band is used for validation tests of the proposed approach.

Dry atmospheric continuum component was not considered in the analysis of our SOLEIL spectra because of its negligible amplitude under the used experimental conditions. However, we briefly mention its modeling in the considered spectral range just to demonstrate the relevance of our general approach.

Dry continuum is mainly associated with the pair interactions involving N_2 and O_2 molecules. The monomolecular component of the dry continuum, related to the deviation of the wings of weak resonance lines (quadrupole transitions in N_2 and magnetic-dipole transitions in O_2) from the Lorentzian profile, can be neglected. Note that in some frequency intervals a contribution of both mono- and bimolecular absorptions from other minor atmospheric gas constituents (such as N_2O, CO_2, CH_4, *etc*.) may also become notable [Karman_2019]. In the range of the H_2O rotational band, dry continuum is dominated by the roto-translational collision-induced bands of N_2 and O_2 pairs. Bimolecular absorption related to transient dipole in O_2 induced by collisions with O_2 and N_2 is much weaker than corresponding absorption in N_2 [Boissoles_Boulet_2003], and thus, the O_2 induced dipole

related component can be neglected at least at the current stage of continuum modeling, where the uncertainty of much more important contributions is large. The N_2-N_2 and N_2-O_2 collision induced spectra are quite similar to each-other [Boissoles_Boulet_2003]. Thus, the dry atmospheric continuum spectrum can be roughly modeled in the considered range using the scaling function from [Boissoles_Boulet_2003] and N_2-N_2 continuum spectrum. As included in the HITRAN database [Karman_2019], the latter is taken from calculations (including contribution of free pairs, stable and metastable dimers) [Karman_2015, Chistikov_2019], which were recently validated by experiment [Serov_Balashov_2020].

As for the wet part of the atmospheric continuum, both self and foreign contributions of bimolecular absorption and the part of monomolecular absorption related to far wings of water resonance lines are significant. It is necessary to take into account three sets of spectra corresponding to all possible pair states of H_2O-*A* (where *A* is any atmospheric molecule), including truly bound (stable dimer), quasibound (metastable dimer) and free pairs. The H_2O-H_2O, H_2O-N_2 and H_2O-O_2 pair states are expected to bring the dominant contributions. Most of these spectra have never been calculated. However, according to estimates obtained in [Svishchev_1998, Vaida_2000, Robinson_2003, Kjaergaard_Robinson_2003, Sabu2005, Baranov_2012], the concentration of the H_2O-N_2 and H_2O-O_2 heterodimers in air (about 10 ppm near the Earth's surface) is much higher than the concentration of gases, such as CH_4, N_2O, CO and various halocarbons which are of principal importance for the calculation of the greenhouse effect of the Earth's atmosphere. Results of the global rotational-vibrational-tunneling absorption spectrum calculations for H_2O-H_2O stable dimer absorption are available for the 0-600 cm^{-1} region [Scribano_2007]. This allows us to illustrate the application of our approach to the self-continuum. The approach is detailed below and will be applied in the future to the foreign-continuum and thus to the total atmospheric absorption modeling.

3.2. *Some specificities of the self-continuum modeling in the range of H_2O rotational band*

As mentioned above, water vapor self-continuum absorption consists of absorption by molecular pairs (including stable and metastable dimer states and neglecting minor contribution of free pairs [Vigasin1991, Leforestier2010, Tretyakov_Sysoev_2015]) and absorption related to far wings of water resonance lines.

The stable water dimer contribution (*BD*) in the 0 – 600 cm^{-1} frequency range is taken into account using results of the *ab initio* calculations of its spectrum [Scribano_2007]. Results of these calculations were validated by more approximate molecular dynamic

approach [Lee_2008] and by experimental observations of the water dimer rotationally resolved spectrum in the 3.5-8.4 cm^{-1} interval [Tretyakov_Serov_2013, Serov_Koshelev_2014]. Stable dimer equilibrium constant K_{BD}, that is related to its dissociation energy and rules its concentration in water vapor at equilibrium conditions was calculated in [Scribano_2006]. However, the value of K_{BD} retrieved from the experimentally observed rotationally resolved spectrum of the dimer at room temperature [Serov_Koshelev_2014] turned out to be lower by about 35 % (0.036 atm^{-1}, that corresponds to 5×10^{-4} relative fraction of stable water dimers in 16 mbar of water vapor) than the calculated value [Scribano_2006]. This difference is explained [Serov_Koshelev_2014] by the fact, that the equilibrium constant calculations (eq. (10) from [Scribano_2006]) involve an overestimated dissociation energy value (1234 cm^{-1}) in comparison with more recent *ab initio* calculations [Leforestier_Szalewicz_2012] and velocity map imaging method [Rocher-Casterline_2011] (1108 cm^{-1} and 1105(10) cm^{-1}, respectively). The experimentally retrieved equilibrium constant K_{BD} = 0.036 atm^{-1} corresponds to a dissociation energy of 1144(19) cm^{-1}, which is in a reasonable agreement with aforementioned values. This K_{BD} value is adopted in the following modeling.

Despite tremendous progress in *ab initio* calculations of bimolecular spectra [Karman_2015], the metastable water dimer (metadimer) absorption spectrum has not been calculated yet because of the very high complexity of this system. Following [Vigasin_2010], we consider two boundary cases to evaluate the spectrum of the water metadimer. In the first extreme case, metastable dimer is a double molecule similar to stable dimer but has a short lifetime. Thus its spectrum is similar to one of stable dimer but homogeneously broadened by the lifetime. Such model was used in [Tretyakov_ Serov_2013, Serov_Koshelev_2014]. In the second extreme case, the metadimer is considered as two monomers almost freely rotating near each other, and its absorption spectrum is approximated by the doubled absorption of the monomer also homogeneously broadened due to the short lifetime of the metastable states. This modeling of metastable dimer spectrum was used in [Odintsova_Tretyakov_2013, Ptashnik_Shine_2011, Serov_Odintsova_2017, Simonova_Ptashnik_2020]. The unknown lifetime broadening *w* is a variable parameter of the model which, in principle, depends on the rovibrational transition. Obviously, neither the first nor the second model can reflect all the characteristics of the metadimer spectrum. For example, in the second one, there will be no characteristic features of the rotation of a pair around its center of mass, and in the first one, the characteristic related to the free rotation of monomers is missing. It is supposed [Vigasin_2010] that metadimer spectrum is intermediate between these two boundary cases

441 and thus can be approximated by a linear superposition of the two boundary cases. This
442 approximation is expected to be good in the range of pure rotational H_2O band because of
443 general similarity of extreme case spectra (both have bell-shape and their intensity maxima
444 coincide).

445 Metadimer equilibrium constant, K_{MD}, can be obtained from the well-established (both
446 experimentally and theoretically) value of the second virial coefficient, $B(T)$ [Stogryn1959,
447 Wagner_Pruss_2002, Leforestier_2014, Tretyakov_Serov_2011]:

448 $$B(T) = b_0 - K_{BD}RT - K_{MD}RT, \quad (11)$$

449 where b_0 is the excluded volume, R is universal gas constant. The excluded volume here
450 represents the part responsible for the free pair states. Empirical approximations of
451 temperature dependences for b_0(T) and B(T) can be found in [Leforestier_2014] and
452 [Tretyakov_Serov_2011], respectively.

453 Keeping in mind the used method of the resonance absorption calculation, the
454 monomolecular component of the total absorption (Eq. (9)) can be written as:

455 $$\alpha_1 = \alpha_R + W \quad (12)$$

456 where W is unknown contribution of an inadequate resonance line shape modeling at large
457 detuning from the line center. The unaccounted in α_R absorption from far wings of resonance
458 lines W is taken into account by a simple model suggested in [Serov_Odintsova_2017]. It uses
459 (similarly to the MT_CKD model) the empirical χ-function modifying Lorentzian wings of
460 resonance lines:

461 $$\chi(v - v_0) = \left(1 + A\frac{|v-v_0|}{dv_{wing}}\right) exp\left(-\frac{(v-v_0)^2}{dv_{wing}^2}\right), \quad (13)$$

462 where v_0 is line center frequency, A and dv_{wing} are variable parameters corresponding to the
463 intermediate wing amplitude and the characteristic width of the wing, respectively. The model
464 takes into account *(i)* known facts that real resonance line is "Lorentzian" and "sub-
465 Lorentzian" in the region of near and far wings, respectively [Clough_1980] and *(ii)* possible
466 "super-Lorentzian" behavior in the range of intermediate wings.

467 The continuum absorption cross-section $C_S^{calc}(T)$ (in $cm^2molec^{-1}atm^{-1}$) can be thus
468 simulated as a sum of contributions of stable and metastable dimer absorption and absorption
469 from far wings of resonance lines:

$$C_S^{calc}(T) = K_{BD}BD(T) + K_{MD}MD(T) + W(T)/P$$

470 $$= K_{BD}D(T) + K_{MD}\left(kMD_1(T) + (1-k)MD_2(T)\right) + W(T)/P, \quad (14)$$

471 where $MD_1(T)$ and $MD_2(T)$ are spectra of metastable dimer according to the first and the
472 second aforementioned extreme cases, respectively, and k is the relative fraction of the first

model of metastable dimer (MD_1) to the total model of metastable dimer spectrum ($0 \leq k \leq 1$). To reduce the number of variable parameters, we fix the shape of the stable dimer spectrum to the calculated one (spectrum curves from Fig. 10 from [Scribano_2007] and the equilibrium constant of stable water dimer to the value listed in **Table 2**. The model of the metastable dimer absorption spectrum includes two variable parameters: the fraction parameter, *k*, and the lifetime, *w*, assumed to be identical for all the transitions. Its equilibrium constant, K_{MD}, was fixed to the value found from the second virial coefficient, as follows from Eq. (11) (see **Table 2**). The far-wing contribution is the most uncertain part and includes two parameters (*A* and dv_{wing}) which are adjusted to the measurements.

The temperature dependence of each continuum component is assumed to follow the power law (at least for the relatively narrow *T*-intervals considered in this work):

$$X(T) = X(T_0)\left(\frac{T_0}{T}\right)^{n_X}, \tag{15}$$

where *X* refers to *BD*, MD_1, MD_2 or *W*, n_X is temperature exponent.

Temperature exponent of the total continuum model is defined as:

$$n = \frac{ln\left(C_S^{calc}(T)/C_S^{calc}(T_0)\right)}{ln\left(T_0/T\right)}. \tag{16}$$

3.3. Model validation versus experimental data

The model function of the continuum absorption cross-section $C_S^{calc}(T)$ including its temperature exponent *n* was optimized to the experimental data available in the range of H_2O rotational band (3.5-600 cm^{-1}), including data from literature [Podobedov_2008, Burch_1981, Burch_Alt_1984, Koshelev_Serov_2011, Kuhn_2002, Liebe_1987, Slocum_2015, Furashov_1996]. We used simultaneous ("multispectrum") fitting of the model to continuum cross-sections at 296 K and 326 K and to the continuum temperature exponent *n*. Final parameters of the model are summarized in **Table 2**. Note, that a change in *A* and *w* with temperature is expected, since both the relative speed of molecular movement and the internal energy increase with temperature. The former leads to the interaction time decrease and, consequently, decrease of possible non-monotonic interaction, which is responsible for the super-Lorenz behavior of wings [Serov_2017]. The latter decreases the average lifetime of metadimers. Contribution of the MD_2 component (like bound) of the metastable dimer spectrum was found to be negligible. This observation supports the choice of

[Ptashnik_Shine_2011, Odintsova_Tretyakov_2013, Serov_Odintsova_2017] to model the metadimer spectrum as a broadened monomer spectrum with double intensity in order to analyze the in-band infrared continuum. On the other hand, it may indicate that the experimental K_{BD} value (0.036 atm^{-1} at 296 K) from [Serov_Koshelev_2014], used in this work, is somewhat overestimated thus confirming conclusions of the work [Buryak_Vigasin_2015], where the equilibrium constant for true bound dimers (equals to 0.016 atm^{-1} at 296 K) was calculated using classical expressions and a complete multidimensional potential energy surface of interacting monomers.

Table 2. Parameters of the continuum model in the rotational band.

	K_{BD}, atm^{-1} [Serov_2014]	K_{MD} [a], atm^{-1}	w [b], cm^{-1}	k [c]	A [d]	dv_{wing} [e], cm^{-1}
296 *K*	0.036	0.016	20	1	19	15
326 *K*	0.017	0.011	30	1	14	15

Notes

[a] Constrained to the value derived from Eq.(11)

[b] Lifetime broadening of metastable dimer spectrum MD_2

[c] Relative fraction of the first model of metastable dimer (MD_1) to the total model of metastable dimer spectrum. Constrained to be identical at 296 K and 326 K

[d] Intermediate line wing amplitude

[e] Characteristic width of the super-Lorentzian part of the line wing. Constrained to be identical at 296 K and 326 K

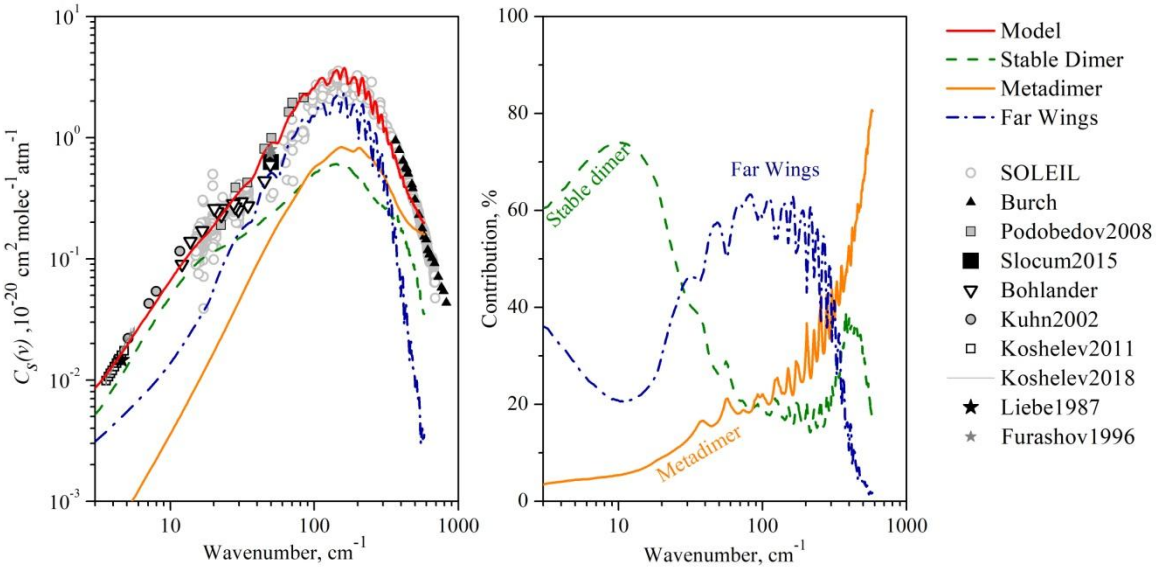

Fig. 2. The self-continuum cross-section (left panel) and relative contribution of continuum components (right panel): grey empty circles: SOLEIL measurements, black triangles: [Burch_1981, Burch_Alt_1984], grey squares: [Podobedov_2008], black star: [Liebe_1987], black empty triangles: measurements of Bohlander [Burch_1981], grey square: [Slocum_2015], grey empty squares: [Koshelev_2011], grey curve: [Koshelev_2018], black circles:

[Kuhn_2002], grey star: [Furashov1996], red solid curve: continuum model, green dash curve: stable dimer model, solid curve: metastable dimer model, blue dash-dot curve: far wings model.

Figure 2 compared the obtained calculated self-continuum at 296 K to the available experimental data. The various contributions are presented separately in absolute (left-hand) and relative (right-hand) scales. An overall good agreement is achieved. Note that the proposed model was constructed in the range up to 600 cm^{-1}, which is limited by the range of calculated data of the bound dimer spectra [Scribano_2007]. For this reason, the data of [Burch_1981, Burch_Alt_1984] above 600 cm^{-1} were not taken into account in the analysis and are shown in **Fig.2** only for comparison. Compared to our measurements, the largest deviations are observed in the 35 – 84 cm^{-1} interval where the calculated values are intermediate between our data and those of [Podobedov_2008]. However, the deviation is within the spread of experimental points.

Temperature exponents – n_{MD_1}, n_{MD_2} and n_W – of the revealed continuum components at experimental temperatures (296 K and 326 K) can be obtained at this step substituting their modeled spectra (MD_1, MD_2 and W, respectively) into the following equation:

$$n_X = \frac{ln\left(X(T)/X(T_0)\right)}{ln\left(T_0/T\right)}. \quad (17)$$

Temperature exponent of stable dimer absorption, n_{BD}, was estimated substituting the results of *ab initio* calculations (Fig. 10 from [Scribano_2007]) at 268 K and 308 K into Eq. (17). The temperature exponent of the total continuum in the range of the pure rotational band is calculated from experimental cross-sections using Eq. (16).

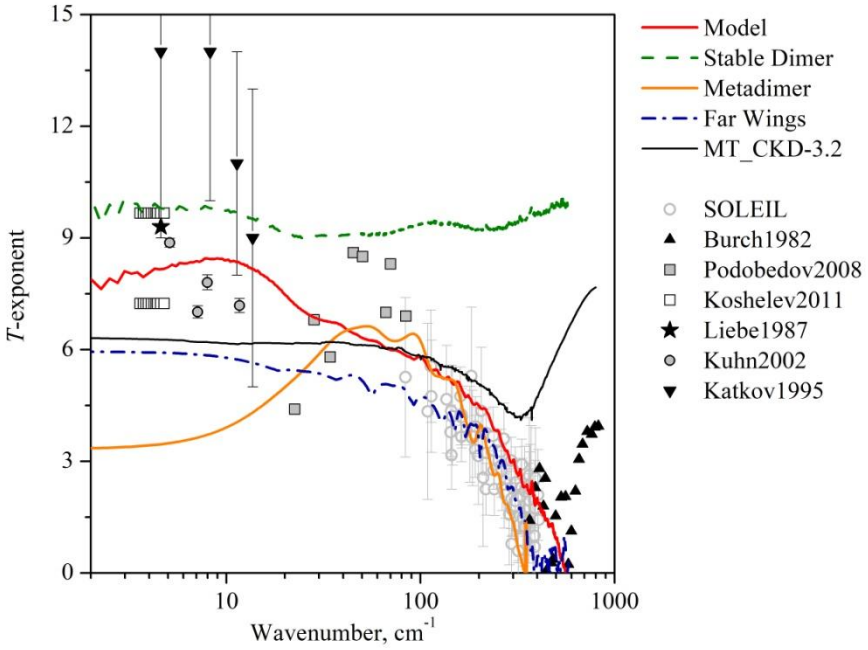

Fig.3. Self-continuum temperature exponent: grey empty circles: SOLEIL measurements, black triangles: [Burch_1981, Burch_Alt_1984], grey squares: [Podobedov_2008], black star: [Liebe_1987], grey empty squares: [Koshelev_2011], black circle: [Kuhn_2002], black triangles: [Katkov_1995], red solid curve: continuum model, green dash curve: stable dimer model, orange solid curve: metastable dimer model MD2, blue dash-dot curve: far wings model, black solid curve: MT_CKD-3.2 model [MT_CKD].

The comparison of the experimental and calculated continuum temperature exponents displayed in **Figure 3** shows an agreement within the spread of experimental points (which is quite significant). Note that the temperature exponents, n_{BD}, n_{MD_1} and n_W are presented separately. Temperature exponent frequency dependence of MT_CKD model qualitatively is very similar to the observed one. However the model overestimates experimental values for frequencies higher than 200 cm^{-1}.

It is worth pointing out that the exclusion of any of the three components from the model significantly worsens the description of the continuum spectrum and its temperature dependence. For example, excluding the contribution of a stable dimer leads to significant underestimation of the continuum in the mm-submm range (10 – 40 cm^{-1}) (see Fig. 2, right-hand). On the other hand, dimer absorption (including stable and metastable states) is insufficient to describe the continuum within whole range of H_2O pure rotational band. This is especially true around the band intensity maximum. A similar conclusion was made from analysis of the in-band continuum in the range of fundamental vibrations [Serov_Odintsova_2017, Ptashnik_2019]. The exclusion of the metadimer contribution from

the model leads to an underestimation of the continuum in the high-frequency wing of the rotational band.

3.4. The self-continuum contributors

Detailed consideration of the continuum in the range of wings and center of the band allowed us to draw some conclusions about its contributors. The mm and sub-mm wave ranges (low frequency wing of the H_2O rotational band) are suitable for the detection of stable dimer spectral signature from spectra recorded at temperatures close to atmospheric. Rotationally resolved water dimer spectrum at close to atmospheric conditions was observed in the 3.5–8.5 cm^{-1} range using resonator spectrometer [Tretyakov_Serov_2013, Serov_Koshelev_2014]. The observed sequence of rotational peaks consists from a large number of overlapped lines (*E*-type transitions) corresponding to the end over end rotation band of the dimer [Krupnov_Tretyakov_2009]. The sequence is predicted to reach a broad maximum located at room temperature around 20 cm^{-1}, corresponding to the range of the most intense rotational transitions [Scribano_2007]. This maximum is expected to be located on a wide absorption pedestal smoothly increasing with frequency, due to the other rotation-tunneling transitions of stable water dimer in the ground and low energy intermolecular vibrational states populated at room temperature. Moreover, similar smooth frequency dependence of metadimers and absorption related to far wing of resonance lines is expected because these absorptions reach their maximum at much higher frequencies. In order to separate absorption related to stable dimer from other sources, the spectral function of the continuum model, $C_S(\nu)/\nu^2$, is considered in this work. The broad absorption maximum due to the dimer rotational absorption near 20 cm^{-1} shows up as a characteristic sharp slope of the spectral function (see **Fig. 4**). Series of continuum measurements in the sub-THz frequency range (15 – 35 cm^{-1}) aimed at detecting this spectral signature were performed at SOLEIL [Odintsova_2017, Odintsova_2019] (see Table 1). Frequency dependence of the registered continuum reproduces the spectral signature of the water continuum predicted by *ab initio* calculations [Scribano_2007]. The available experimental data on the continuum spectral function displayed in **Fig. 4** show an overall satisfactory agreement with the model.

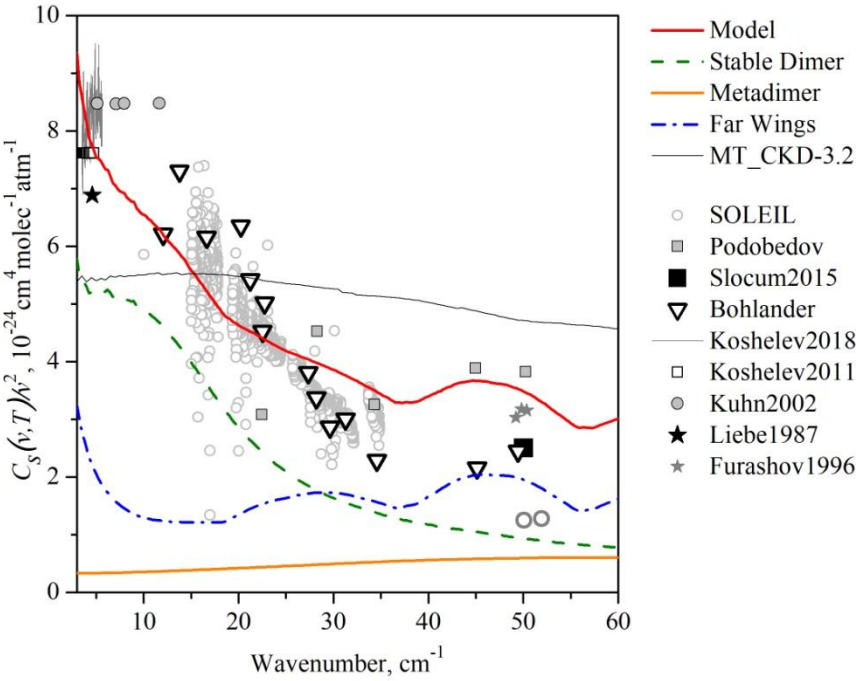

Fig.4. Continuum spectral function: grey empty circles: SOLEIL measurements [Odintsova_2019, Odintsova_2017], black empty triangles: [Burch_1981], grey squares: [Podobedov_2008], grey curve:[Koshelev_2018], grey empty squares: [Koshelev_2011], grey filled circles: [Kuhn_2002], grey star: [Furashov1996], green dash curve: stable dimer model, orange solid curve: metastable dimer model MD_2, blue dash-dot curve: far wings, red solid curve: resulting continuum model, black thin curve: MT_CKD-3.2 model.

In the 15 – 35 cm^{-1} range, the relative contribution of the stable dimer absorption to the continuum is estimated to be about 50 – 75 %. According to our model, relative contributions of the metadimer absorption and "non-Lorentzian" far wings of resonance water lines are comparable and significantly lower. Note that the increase of the modeled spectral function of far wings in the mm wave range (<5 cm^{-1}) is probably a consequence of the model approximations and should be taken with caution. The analysis of the temperature dependence (**Fig. 3**) in the mm and sub-mm wave ranges indicates that the temperature exponent of the model (which is within 7 – 8) is very close to that of stable water dimer (about 9 – 10) [Odintsova_2020].This confirms that stable dimers bring the dominant contribution in this range.

As illustrated in **Fig.2 (righ-hand)**, the contribution of stable dimer absorption to the continuum decreases to 20 % in the range of band intensity maximum (100 – 300 cm^{-1}), while the metadimer contribution increases with frequency from 20 to 40 %. The remaining 40 – 60 % is attributed to "non-Lorentzian" far wings of resonance water lines. In the high-frequency wing (300 – 600 cm^{-1}), metadimer contribution is dominant (40 to 80 % of the total

absorption) while stable dimer contribute by about 20 – 35 % and the far wings contribution decreases with frequency from 40 to about 2 %.

A similar conclusion is obtained from the temperature dependence (**Fig.3**). The exponent value decreases from 7 – 9 below 50 cm^{-1} to 2 around 300 cm^{-1}. Modeled values of the exponent *n* related to metadimers and non-Lorentzian wings demonstrates similar behavior, but calculated values of *n* related to the stable dimers [Scribano_2007] remain high and almost constant. The temperature dependence thus confirms that the relative contribution of the bound dimer decreases with wavenumber while the contribution of non-Lorentzian wings and metadimers become significant.

4. Discussion and conclusions

SOLEIL's experimental data on water vapor continuum reported in [Odintsova_2017, Odintsova_2019, Odintsova_2020, Koroleva_2021] have been reviewed and analyzed, that allowed advancing in quantitative characterization and general understanding of the continuum. In particular, the relative contribution of the stable and metastable dimer absorption and far wings of resonance lines has been evaluated in the range of the wings and center of the H_2O rotational band. A physically based modeling of the atmospheric continuum is proposed and tested with the water self-continuum in the 0-600 cm^{-1} range. The proposed model of the self-continuum, which explicitly takes into account all significant mechanisms, is in a qualitatively good agreement with the observed spectra. Semi-empirical description of non-Lorentzian wings of resonance lines and spectrum of metastable pair states are the major uncertainties of this model. A more accurate description of the wings of resonance lines can be achieved, in our opinion, on the basis of semi-classical trajectory based calculations [Chistikov_2019, Chistikov_2021]. Currently, this method allows calculating bimolecular absorption by non-polar molecules. The extension of the method to molecules possessing a permanent dipole moment will allow the proper calculation of super- and sub-Lorentzian wings of resonance lines. The same approach appears the most promising for approximate calculations of the metadimer spectra until accurate quantum chemical calculations become available. Note that the reproduction of calculations of the bound dimer spectrum either by the trajectory or by quantum chemical method with the use of an improved potential energy surface of the dimer is also much desired, as well as experimental and theoretical verification of the bound dimer equilibrium constant.

Acknowledgments

This work becomes possible due to the Project Nos. 20140227, 20180347 and 20170067 supported by Soleil Synchrotron. O. Pirali from SOLEIL is warmly acknowledged for his help during the FTS recordings. The work was performed under partial financial support from the State Project No. 0030-2021-0016. SA acknowledges support from the Ministry of Science and High Education of the Russian Federation (Program of the Basic Scientific Investigations, budget funds for IAO SB RAS, Project No. 121031500297-3).

References

[Sizov_2010] F. Sizov, A. Rogalski, Prog. Quantum Electron. 34(5) (2010) 278-347.

[Consolino_2017] L. Consolino, S.Bartalini, P.De Natale, J. Infrared Millim. Te. 38 (2017) 1289–1315.

[MT_CKD] E.J. Mlawer, V.H. Payne, J.L. Moncet, J.S. Delamere, M.J. Alvarado, D.C. Tobin, , Philos. Trans. R. Soc. A Math. Phys. Eng. Sci. 370 (2012) 2520–2556.

[Odintsova_2017] T. A. Odintsova, M. Yu. Tretyakov, O. Pirali, P. Roy,J. Quant. Spectrosc. Rad. Transf. 187 (2017) 116–123.

[Odintsova_2019] T.A. Odintsova, M.Yu. Tretyakov, A.O. ZibarovaO.Pirali, P. Roy, A. Campargue, J. Quant. Spectrosc. Rad. Transf. 227 (2019) 190–200.

[Odintsova_2020] T. A. Odintsova, M. Yu. Tretyakov, A. A. Simonova, I. V. Ptashnik, O. Pirali, A. Campargue, J. Mol. Structure. 1210 (2020) 128046.

[Koroleva_2021] A.O. Koroleva, T.A. Odintsova, M.Yu. Tretyakov, O. Pirali, A. Campargue, J. Quant. Spectrosc. Rad. Transf.261 (2021) 107486.

[Vigasin_2003] Weakly Interacting Molecular Pairs: Unconventional Absorbers of Radiation in the Atmosphere / ed. by C. Camy-Peyret and A. A. Vigasin. — Dordrecht : Kluwer Academic, 2003. — 287 p. — (NATO ARW Proceedings Series).

[Boissoles_Boulet_2003] J. Boissoles, C. Boulet, R.H. Tipping, A. Brown, Q. Ma, J Quant. Spectr. Radiat. Transf. 82 (2003) 505–516.

[Serov_Balashov _2020] E.A. Serov, A.A. Balashov, M.Yu. Tretyakov, T.A. Odintsova, M.A. Koshelev, D.N. Chistikov, A. A. Finenko, S. E. Lokshtanov, S.V. Petrov, A.A. Vigasin, J. Quant. Spectrosc. Rad. Transf. 242 (2020) 106774

[Vigasin_1991] A.A. Vigasin, Infrared Phys. 32 (1991) 451–470.

[Leforestier_2010]Leforestier C, Tipping RH, Ma Q, J. Chem. Phys. 132 (2010) 164302.

[Tretyakov_2015] M.Yu.Tretyakov, A.A. Sisoev,T.A. Odintsova, A.A. Kyuberis,Radiophysics and Quantum Electronics. (2015) 58(4) 262-276.

[Ma_Tipping_Leforestier_2008]Q. Ma, R.H. Tipping, C. Leforestier,J. Chem. Phys.128 (2008) 124313.

669 [Elsasser_1938] W. M. Elsasser, Phys. Rev. 54 (1938) 126–129.

670 [Serov_Odintsova_2017] E. A. Serov, T.A. Odintsova, M. Yu. Tretyakov, and V.E. Semenov,
671 J. Quant. Spectrosc. Rad. Transf. 193 (2017) 1-12.

672 [Tvorogov_Nesmelova_1994] S. D. Tvorogov, L. I. Nesmelova, O.B. Rodimova, Atmos.
673 Ocean. Phys. 7(11–12) (1994) 802.

674 [Klimeshina_2015] T. E. Klimeshina, O. B. Rodimova, J. Quant. Spectrosc. Rad. Transf.161
675 (2015) 145–152.

676 [Clough_1989] S. Clough, F. Kneizys, R. Davies, Line shape and water vapor continuum,
677 Atmos. Res. 23 (1989) 229–241.

678 [Tretyakov _ Serov _2013] M.Yu. Tretyakov, E.A. Serov, M.A. Koshelev, V.V. Parshin, A.F.
679 Krupnov, Phys. Rev. Lett. 110 (2013)093001

680 [Serov_Koshelev_2014] E.A. Serov, M.A. Koshelev, T.A. Odintsova, V.V. Parshin, and
681 M.Yu.Tretyakov,Phys. Chem. Chem. Phys. 16 (47) (2014) 26221 – 26233.

682 [Ptashnik_Shine_2011] I.V. Ptashnik, K.P. Shine, A.A. Vigasin, J. Quant. Spectrosc. Rad.
683 Transf. 112 (2011) 1286-1303.

684 [Birk_2020] M. Birk, G. Wagner, J. Loos J, K.P. Shine J.Quant. Spectrosc. Rad. Transf. 253
685 (2020)107134.

686 [Scribano_2007] Y. Scribano, C. Leforestier, J. Chem. Phys. 126 (2007)234301.

687 [Kjaergaard_2008] H.G. Kjaergaard, A.L. Garden, G. M. Chaban, R.B. Gerber, D.A.
688 Matthews, J. F. Stanton, J. Phys. Chem. A 112(18) (2008) 4324–4335

689 [Salmi_2008] T. Salmi, V. Hänninen, A.L Garden, H.G. Kjaergaard, J. Tennyson, L. Halonen,
690 J. Phys. Chem. A. 112(28) (2008) 6305-6312

691 [HITRAN2016] I. E. Gordon et al, J. Quant. Spectrosc. Rad. Transf. 203 (2017) 3–69

692 [VanWleck_ Huber_1977] J.H. Van Wleck, D.L. Huber, Reviews of Modern Physics,
693 49(4)(1977) 939-959

694 [Golubiatnikov_2006]G.Yu.Golubiatnikov,V.N. Markov,A.Guarnieri,R. Knoechel, J. Mol.
695 Spectrosc. 240 (2006) 251–254.

696 [Golubiatnikov_2005] G. Yu.Golubiatnikov, J. Mol. Spectrosc. 230 (2005) 196–198.

697 [Golubiatnikov_2008] G. Yu.Golubiatnikov,M. A.Koshelev,A. F.Krupnov, J.
698 Quant.Spectrosc. Radiat. Transf. 109 (2008) 1828–33.

699 [Koshelev_2011] M. A. Koshelev, J. Quant. Spectrosc. Radiat. Transf. 112 (2011) 550–552.

[Koshelev_2007] M. A.Koshelev,M. Yu.Tretyakov,G. Yu.Golubiatnikov,V.V. Parshin, V.N. Markov,I. A.Koval, J. Mol.Spectrosc. 241 (2007) 101–108.

[Tretyakov_2013] M.Yu.Tretyakov,M. A.Koshelev,I. N.Vilkov,V. V.Parshin,E. A. Serov, J. Quant. Spectrosc. Radiat. Transf. 114 (2013) 109–121.

[Podobedov_2008] V. B. Podobedov, D.F. Plusquellic, K. E. Siegrist, G.T. Fraser, Q. Ma, R. H. Tipping, J. Quant. Spectrosc. Radiat. Transf. 109 (2008) 458–467.

[Burch_1981]D. Burch, Atmos. Transm. 277 (1981) 28–39.

[Burch_Alt _1984]D. E. Burch, R.L.Alt,US Air Force Geophysics Laboratory report AFGL-TR-84–0128, Hanscom Air Force Base, MA, USA(1984)

[Campargue_Kassi_2016] A. Campargue, S. Kassi, D. Mondelain, S. S. Vasilchenko, D. Romanini, J. Geophys. Res. Atmos. 121(21) (2016) 13180-13203.

[Bauer_1998] A. Bauer, M. Godon, J. Carlier, R.R. Gamache, J. Quant. Spectrosc.Radiat. Transfer.59(3-5) (1998) 273-85.

[Koshelev_Serov_2011] M.A. Koshelev, E.A. Serov, V.V. Parshin, M.Yu. Tretyakov, J. Quant. Spectr. Radiat. Transf. 112 (2011) 2704–2712.

[Liebe_1897] H.J. Liebe, D.H. Layton, NTIA Rep. (1987) 87–224.

[Kuhn_2002] T. Kuhn, A. Bauer, M. Godon, S. Buehler, K. Kuenzi, J. Quant. Spectrosc. Radiat. Transf. 74 (2002) 545–562.

[Ptashnik_2019] I. V. Ptashnik et al., J. Quant. Spectrosc. Radiat. Transf. 228 (2019) 97–105.

[Vigasin_2000] A. A. Vigasin, J. Quant. Spectrosc. Radiat. Transf.64 (1) (2000) 25-40.

[Slocum_2015]D. Slocum, R. Giles, T. Goyette, J. Quant. Spectrosc. Radiat. Transf. 159 (2015) 69–79.

[Furashov_1996] N.I. Furashov, B. A. Sverdlov, S.N. Chernyaev, Radiophysics and Quantum electronics. 39(9) (1996) 754-9.

[Kwon_2021] J.-G. Kwon, M.-W. Park, T.-I. Jeon, J. Quant. Spectrosc. Radiat. Transf. 272 (2021) 107811.

[Yang_2014] Y. Yang, M. Mandehgar, D. Grischkowsky, Opt. Express. 22 (4) (2014) 4403

[Pardo_2001] J.R. Pardo, E. Serabyn, J. Cernicharo, J. Quant. Spectrosc. Rad. Transf. 68 (2001) 419-433

[Alvarado_Payne_2013] M. J. Alvarado, V. H. Payne, E. J. Mlawer, G. Uymin, M. W. Shephard , K. E. Cady-Pereira, J. S. Delamere, J.-L. Moncet, Atmos. Chem. Phys., 13, 6687–6711, 2013

[Lechevallier_2018] L.Lechevallier, S.Vasilchenko, R.Grilli, D.Mondelain, D. Romanini, A.Campargue, Atmos. Meas. Tech. 11 (2018) 2159–2171.

[Baranov_2011]. Yu. I. Baranov, W. J. Lafferty, Quant. Spectrosc. Rad. Transf. 112 (2011) 1304–1313.

[Simonova_2022] A.A.Simonova, I.V.Ptashnik, J. Elsey, R. A.McPheat, K.P.Shine, K.M.Smith, J.Quant. Spectrosc. Rad. Transf. 277 (2022) 107957.

[Karman_2019] T. Karman et al., Icarus. 328 (2019) 160-175.

[Karman_2015] T. Karman, E. Miliordos, K.L.C. Hunt, G.C. Groenenboom, A. van der Avoird, J. Chem. Phys., 142 (2015) 084306

[Chistikov_2019] D. N. Chistikov et al. J. Chem. Phys. 151(2019) 194106

[Svishchev_1998] I.M. Svishchev, R.J. Boyd, J. Phys. Chem. A. 102(1998) 7294-7296.

[Vaida_2000] V. Vaida, J.E. Headrick. J. Phys. Chem. A. 104(23)(2000) 5401-5412

[Robinson_2003] T.W. Robinson, H.G. Kjaergaard, J. Chem. Phys. 119(2003) 3717-3720

[Kjaergaard_Robinson_2003] H.G. Kjaergaard, T.W. Robinson, D.L. Howard, J. Phys. Chem. A. 107 (2003) 10680-10686

[Sabu_2005] A. Sabu, S. Kondo, R. Saito, Y. Kasai, K. Hashimoto, J. Phys. Chem. A. 109(2005) 1836-1842.

[Baranov_2012] Yu. I. Baranov, I. A. Buryak, S. E. Lokshtanov, V. A. Lukyanchenko, A. A. Vigasin, Phil. Trans. R. Soc. A. 370 (2012) 2691-2709.

[Lee_2008] M.-S. Lee, F. Baletto, D.G. Kanhere, S. Scandolo, J. Chem. Phys. 128 (2008) 214506

[Scribano_2006] Y. Scribano, N. Goldman, R.J. Saykally, C. Leforestier, J. Phys. Chem. A. 110 (2006) 5411-5419

[Leforestier_Szalewicz_2012] C.Leforestier, K.Szalewicz, A. van der Avoird, J. Chem. Phys. 137 (2012) 014305

[Rocher-Casterline_2011] B. E. Rocher-Casterline, A. K. Mollner, L. C. Ch’ng, H. Reisler, J. Phys. Chem. A. 115 (2011) 6903–6909

[Vigasin_2010] A. A.Vigasin, Mol. Phys. 108 (2010) 2309–2313.

[Odintsova_Tretyakov _2013] T. A. Odintsova, M. Yu. Tretyakov, J. Quant. Spectrosc. Rad. Transf. 120 (2013) 134-137.

[Simonova_Ptashnik_2020] A.A. Simonova, I.V.Ptashnik, Proc. SPIE. 1156002 (2020) 1–7.

[Stogryn1959] D. E. Stogryn and J. O. Hirschfelder, J. Chem. Phys., 31. 6 (1959) 1531-1545

[Wagner_Pruss_2002] W.Wagner and A. Pruss, J. Phys. Chem. Ref. Data, 31(2002) 387.

[Tretyakov_ Serov_2011] M.Yu. Tretyakov, E.A. Serov, T.A. Odintsova, Radiophysics and Quantum Electronics, 54 (10) (2012) 700–716.

[Leforestier_2014] C. Leforestier. J. Chem. Phys. 140 (2014)074106

[Hirschfelder_1942] J. O. Hirschfelder, F. T. McClure, I. F. Weeks, J. Chem. Phys. 10 (1942) 201.

[Clough_1980] S.A. Clough, F.X.Kneizys, R. Davies,R.Gamache, R.Tipping, Theoretical lineshape for H2O vapor; application to the continuum. In: Deepak A, Wilkerson TD, Ruhnke LH, editors. Atmospheric water vapor. NewYork: AcademicPress; (1980) 25.

[Odintsova_Tretyakov_2013] T. A.Odintsova, M.Yu.Tretyakov, J. Quant.Spectrosc.Radiat. Transfer. 120 (2013) 134-137.

[Buryak_Vigasin_2015] I. Buryak, A.A. Vigasin. J. Chem. Phys. 143, 234304 (2015).

[Krupnov_Tretyakov_2009] A.F. Krupnov, M.Yu. Tretyakov, C. Leforestier, J. Quant. Spectrosc. Rad. Trans. 110 (2009) 427–434

[Chistikov_2021] D. N. Chistikov et al. J. Chem. Phys. 155(6) (2021)064301